A METHOD FOR COMPUTING THE PRESSURE DISTRIBUTION ABOUT AN AXISYMMETRIC NACELLE IN SUBSONIC FLOW

by

Darryl Jon Trulin

A Dissertation Submitted to the

Graduate Faculty in Partial Fulfillment of

The Requirements for the Degree of

DOCTOR OF PHILOSOPHY

Major Subjects: Aerospace Engineering
Mechanical Engineering

Approved:

Signature was redacted for privacy.

In Charge of Major Work

Signature was redacted for privacy.

Heads of Major Departments

Signature was redacted for privacy.

Dean of Graduate College

Iowa State University
Of Science and Technology
Ames, Iowa

1968

TABLE OF CONTENTS

INTRODUCTION

Design Considerations for Axisymmetric Nacelles

In the design of an aircraft utilizing an air-breathing engine that is not located within the airframe, the flow field characteristics about the engine cowling or nacelle must be known. The primary function of this nacelle is to provide an adequate supply of air to the engine and to present a smooth surface and minimum resistance to the external air flow.

Several other considerations are involved in the design of an engine nacelle. For example, a pressure force integration over the forward portion of a modern jet nacelle shows that this pressure force contributes a sizable portion of the engine's thrust. Therefore, care must be taken to insure that undesirable conditions that might reduce this thrust, such as separation in the diffuser, do not occur. Experience has shown that nacelle shapes which cause the air to accelerate rapidly over the outer surface lip with an accompanying low pressure "spike" will experience local supersonic flows with their inherent shocks and drag rise at low Mach numbers. Then, if the pressure is found to have a fast recovery over the outer surface in the aft end of the nacelle, these flows will often tend to separate with a resulting increase in the drag. In addition, a viscous analysis of the flow field is also necessary to accurately predict the drag. Many methods of estimating drag first require a knowledge of the inviscid flow solution about the nacelle.

Historical Background

Early nacelles and cowls were designed by using airfoil sections to define their outline. Probably the most well-known group of experimental cowls is the NACA 1-series found in References (1), (2), and (3). Unfortunately, these inlet shapes had very sharp lips and do not perform well for jet engine applications. The design of later cowl shapes was guided by experience and a trial-and-error system of experimental testing of various shapes by individual companies. This particular thesis had its origin in work done at the Boeing Company in Seattle, Washington. A digital computer program was developed at Boeing (4) utilizing a series of vortex rings in a uniform flow to generate the nacelle surface. Although the program was used a great deal, it had several serious flaws. As originally developed, the program was not successful in predicting the pressure variation about a thin cowl, and the results obtained were extremely sensitive to the location and spacing of the rings. Even when great care was used in defining the nacelle surface, the resulting pressure distribution predicted by the program was often an unrealistic saw-tooth pattern. Other early airfoil programs also used discrete singularities similar to the ring vortex and with them the user experienced a similar problem. This problem was eliminated by spreading out the concentrated singularity strength over a surface area to form a sheet across which the velocity could be discontinuous.

This particular thesis is a three-dimensional extension of the last of the above mentioned two-dimensional airfoil programs in that the concentrated vortex ring singularity is spread over an axisymmetric surface.

Smith and Pierce (5) have developed a computer program using source and sink surfaces of constant strength in an incompressible, nonviscous flow field to predict the flow characteristics about a body. This program has been used to solve many different aerodynamic problems but did experience difficulty with a thin cowl of finite length. If only sources and sinks are used, one cannot generate any circulation about the nacelle cross section and the Kutta condition at the trailing edge cannot be satisfied.

Several other methods of solution are currently being used. One of the most successful is the relaxation scheme described in such references as (6) and (7), and this method has been programmed for the digital computer (8). Although this method does have the advantage of being able to solve the compressible case, it still suffers from the requirement of a somewhat tedious input. Relaxation methods are always time consuming and require large computer storage space and, therefore, are rather costly in terms of computer usage. A comparison of the relative merits of the Boeing ring program and the relaxation program can be found in Reference (9).

In this thesis a simple tool for axisymmetric nacelle analysis is developed. For simplification purposes the problem is restricted to a steady, inviscid, incompressible fluid flow about an axisymmetric nacelle at zero angle of attack. In the mathematical representation the nacelle is replaced by a surface of vorticity defining the body shape with a superimposed uniform flow. As usual, the boundary conditions require tangential flow at the body surface and a modified Kutta condition at the trailing edge. A result is that the inputs are easily prepared and the run time on the IBM 360-65 computer is usually less than one minute. The output from the main computer program consists of the pressure coefficients and velocity

components at points on the nacelle surface. In addition to the main program, there are two subroutines that increase the applicability of the total program. The first incorporates a subsonic Gothert rule correction to predict the effect of compressibility on the pressure coefficients. This subroutine requires the desired freestream Mach number as an additional input. The second subroutine allows the user to select points off the nacelle and the output consists of pressure and velocity at these field points.

LIST OF SYMBOLS

Variables

C_p = Pressure coefficient

$cogs_{2n-1}$ = Coefficient of δ_{2n-1} term in Equation (41) used to express circulation about torus cross section

$cogu_{2n-1}$ = Coefficient of δ_{2n-1} term in axial velocity equation (36)

$cogv_{2n-1}$ = Coefficient of δ_{2n-1} term in radial velocity equation (37)

E = Elliptic integral of the second kind

k = Modulus of the elliptic integrals

k' = Complementary modulus of the elliptic integrals

K = Elliptic integral of the first kind

$\bar{l}$ = Vector arc length of an increment of a vortex filament

L = Vortex sheet length

M = Mach number

M_{21}, M'_{21} = Coefficients of δ_3 and δ_1 in axial velocity equation (34) for a single frustum

N_{21}, N'_{21} = Coefficients of δ_3 and δ_1 in radial velocity equation (35) for a single frustum

p = Static pressure

q = Dynamic pressure

Q_{2n-1} = Coefficient of δ_{2n-1} term in tangential flow boundary condition equation (40)

r = Radial coordinate of a field point

r' = Radius of a ring vortex

R = Dimensionless radius of a ring vortex

$\bar{R}$ = Radius vector from a vortex filament to a field point

s = Surface length of a frustum

S = Dimensionless surface length of a frustum

u = Axial velocity component

v = Radial velocity component

V = Magnitude of fluid velocity

$\bar{V}$ = Fluid velocity

x = Streamwise coordinate locating points from ring vortex

x' = Streamwise coordinate locating ring vortex

X = Dimensionless axial length from a ring vortex to the frustum midpoint

y = Cartesian coordinate

α = Variable of integration in the elliptic integrals

α = Angle of attack

β = Slope angle of the frustum surface

δ = Surface vortex strength of a sheet of vorticity

Γ = Circulation of a vortex filament

θ = Angle between ρ' and the x axis

ξ = Dummy variable of integration

ρ = Density

ρ' = Distance from field point to a vortex sheet

Φ = Velocity potential

Subscripts

I = Inlet conditions

∞ = Freestream conditions

DERIVATION OF VELOCITY EQUATIONS

Velocity at a Field Point Due to a Ring Vortex

The steady state flow of a continuous, irrotational, incompressible, inviscid fluid can, in part, be expressed by the following kinematic equation

$$\nabla^2 \Phi = 0 \tag{1}$$

where Φ is the velocity potential. Since this differential equation is linear, a superposition of simple flows that satisfy the above Laplace equation and the boundary conditions may be used to represent more complex flow problems. One such simple flow is that of the vortex filament described in (10). The equation expressing the velocity field due to an element of the vortex filament in terms of its circulation Γ is the Biot-Savart law (11).

$$d\bar{V} = \frac{\Gamma(\bar{R} \times d\bar{l})}{4\pi |\bar{R}|^3} \tag{2}$$

The geometry expressed in this equation for an increment of the particular vortex filament used in axially symmetric flow, the ring vortex, is shown in Figure 1. The Biot-Savart equation is well defined for all points P not on the increment, and these points will be referred to as field points. The axial and radial velocity components at a field point P due to the ring vortex in Figure 1 are obtained by integrating Equation 2 around the ring. This integration, outlined by Kuchemann and Weber (12), yields the component equations

$$u = \frac{\Gamma}{2\pi\left[x^2+(r+r')^2\right]^{\frac{1}{2}}}\left\{K-E\left[1+\frac{2(r-r')r'}{x^2+(r-r')^2}\right]\right\} \tag{3}$$

$$v = \frac{-x\Gamma}{2\pi r\left[x^2+(r+r')^2\right]^{\frac{1}{2}}}\left\{K-E\left[1+\frac{2rr'}{x^2+(r-r')^2}\right]\right\} \tag{4}$$

In these equations K and E are elliptic integrals and are defined along with their modulus k by the following equations:

$$K = \int_0^{\pi/2} \frac{d\alpha}{\left[1-k^2\sin^2\alpha\right]^{\frac{1}{2}}} \tag{5}$$

$$E = \int_0^{\pi/2} \left[1-k^2\sin^2\alpha\right]^{\frac{1}{2}} d\alpha \tag{6}$$

$$k^2 = \frac{4rr'}{x^2+(r+r')^2} \tag{7}$$

Velocity at a Field Point Due to a Frustum of Linearly Varying Vorticity

The approximation that is used in this study involves the replacement of the double-curved surfaces of the nacelle with many frustum surfaces as shown in Figure 2. In the mathematical representation of the physical flow, these frustum surfaces will be sheets of vorticity whose strength is such that the fluid flows tangentially to these frustum surfaces when placed in a uniform flow field.

Since the flow is axially symmetric, the vorticity is the same for all points on a given elementary ring of a frustum. That is, for points on a given ring, located by an axial and radial dimension, the vorticity is not a function of the angular dimension in the cylindrical coordinate system used.

Several constraints are placed on the allowable variation of vorticity in this development. To simplify the mathematics involved, the vorticity will be restricted to a linear variation along the surface on a given frustum. This variation of vorticity as a function of surface length s is illustrated by the annular torus in Figure 3 and Figure 4.

The basic element of vorticity on the frustum is the ring vortex shown in Figure 5. Its circulation $d\Gamma$ is equal to the product of the surface vortex strength times a differential surface length.

$$d\Gamma = \gamma\, ds \tag{8}$$

Since the only vorticity variation to be allowed on a frustum is a linear variation with the surface length, the surface vortex strength γ can be written in terms of the vorticity at the frustum bases or corners and the surface length s to that ring.

$$\gamma = \left[\frac{\gamma_2-\gamma_1}{s_2-s_1}\right]\left[s-s_1\right]+\gamma_1 \tag{9}$$

The total effect of the frustum of vorticity shown in Figure 5 at the field point P requires the integration of the differential form of the ring equations 3 and 4 with respect to the surface length s between the limits s_1 and s_2.

$$u = \int_{s_1}^{s_2} \frac{\gamma}{2\pi\left[x^2+(r+r')^2\right]^{\frac{1}{2}}} \left\{K-E\left[1 + \frac{2(r-r')r'}{x^2+(r-r')^2}\right]\right\} ds \tag{10}$$

$$v = \int_{s_1}^{s_2} \frac{\gamma\ (=x)}{2\pi r\left[x^2+(r+r')^2\right]^{\frac{1}{2}}} \left\{K-E\left[1 + \frac{2rr'}{x^2+(r-r')^2}\right]\right\} ds \tag{11}$$

These equations can then be written in terms of the vorticity at the frustum corners by using Equation 9.

$$u = \frac{(\gamma_2-\gamma_1)}{2\pi(s_2-s_1)} \int_{s_1}^{s_2} \frac{s}{\left[x^2+(r+r')^2\right]^{\frac{1}{2}}} \left\{K-E\left[1 + \frac{2r'(r-r')}{x^2+(r-r')^2}\right]\right\} ds$$

$$- \frac{(\gamma_2 s_1-\gamma_1 s_2)}{2\pi(s_2-s_1)} \int_{s_1}^{s_2} \frac{1}{\left[x^2+(r+r')^2\right]^{\frac{1}{2}}} \left\{K-E\left[1 + \frac{2r'(r-r')}{x^2+(r-r')^2}\right]\right\} ds \tag{12}$$

$$v = \frac{(-\gamma_2+\gamma_1)}{2\pi r(s_2-s_1)} \int_{s_1}^{s_2} \frac{x(s)}{\left[x^2+(r+r')^2\right]^{\frac{1}{2}}} \left\{K-E\left[1 + \frac{2rr'}{x^2+(r-r')^2}\right]\right\} ds$$

$$+ \frac{(\gamma_2 s_1-\gamma_1 s_2)}{2\pi r(s_2-s_1)} \int_{s_1}^{s_2} \frac{x}{\left[x^2+(r+r')^2\right]^{\frac{1}{2}}} \left\{K-E\left[1 + \frac{2rr'}{x^2+(r-r')^2}\right]\right\} ds \tag{13}$$

Equations 12 and 13 express the axial and radial velocity components at a field point due to a frustum of linearly varying vorticity. If the geometry of this simple example is known, the integrations can be performed and the velocity components are then merely functions of the surface vortex strengths γ_1 and γ_2 at the frustum corners.

Velocity Components at the Midpoint of a Frustum with Linearly Varying Vorticity

In the previous section the velocity component equations at a field point due to a frustum of vorticity were derived. In this section the point examined is not a field point but rather a singular point on the frustum and, in particular, the midpoint of that surface. The analysis will be done in two parts. As described in Reference (11), a vortex sheet will support a discontinuity in tangential velocity while the normal velocity is continuous through the sheet. In the first part of the analysis the midpoint will not be specified as being on the inner or outer surface of the frustum. Therefore, in this incomplete analysis the phenomenon of discontinuous velocity does not appear. In the second part of the analysis the contribution of the local surface vortex strength is examined, and it is this entity that generates the discontinuity in the velocity.

The basic vorticity element is again the ring vortex as shown in Figure 6. The same velocity component equations 10 and 11 are valid but are improper integrals for points on the frustum surface. To evaluate these integrals the method employed by Smith (5) is used.

The orientation of the coordinate system used in the derivation of the singular point velocity equations is chosen to take advantage of the geometry

of this special case. Since the singular point in question is always the midpoint of the frustum surface, the origin will be located at this axial position as shown in Figure 6. The coordinates are nondimensionalized by using the radius of the frustum surface midpoint as a divisor.

$$r = \text{constant} \tag{14}$$

$$S = \frac{s}{r} \tag{15}$$

$$X = \frac{s}{r} \cos \beta$$

or

$$X = S \cos \beta \tag{16}$$

$$R = \frac{r'}{r} = \frac{r+s \sin \beta}{r}$$

or

$$R = 1 + S \sin \beta \tag{17}$$

With the coordinate system described, the frustum surface integration will have a lower limit of $-S_1$ and an upper limit of S_1 where S_1 is half the nondimensional surface length. This simplifies the integration as the integral of odd functions will be zero and the integral of even functions will have a value twice that of the integral from the origin to S_1. Equations 10 and 11 can now be written in terms of these dimensionless parameters as

$$u = \int_{-S_1}^{S_1} \frac{\gamma}{2\pi\left[X^2+(1+R)^2\right]^{1/2}} \left\{ K-E\left[1 + \frac{2(1-R)R}{X^2+(1-R)^2}\right]\right\} dS \tag{18}$$

and

$$v = \int_{-S_1}^{S_1} \frac{(-X)\,\gamma}{2\pi\left[X^2+(1+R)^2\right]^{\frac{1}{2}}} \left\{ K - E\left[1 + \frac{2R}{X^2+(1-R)^2} \right] \right\} dS \qquad (19)$$

To evaluate the integrals each term in the integrands will be expressed as a power series in S.

The frustum geometry will be chosen such that the maximum magnitude of S will be less than 0.1 so that the desired multiplication of the power series may be performed and the resulting product, an infinite series, may be truncated to include only the terms having small integer powers of S.

To obtain a power series expansion in S for the elliptic integrals K and E, they are first expressed in series form as a function of their complementary modulus k' as given by Jahnke and Emde (13).

$$K = \left[\ln \frac{4}{k'} \right] \left[1 + \frac{k'^2}{4} + \frac{9}{64} k'^4 + \frac{25}{256} k'^6 + \ldots \right] - \left[\frac{k'^2}{4} + \frac{21}{128} k'^4 + \frac{185}{1536} k'^6 + \ldots \right] \qquad (20)$$

$$E = \left[\ln \frac{4}{k'} \right] \left[\frac{k'^2}{2} + \frac{3}{16} k'^4 + \frac{15}{128} k'^6 + \ldots \right] + 1 - \frac{1}{4} k'^2 - \frac{13}{64} k'^4 - \frac{9}{64} k'^6 + \ldots \qquad (21)$$

$$k'^2 = 1 - k^2 \qquad (22)$$

The next step consists of writing the complementary modulus k' as a function of S. To do this, the modulus in Equation 22 is replaced by its equivalent

function from Equation 7 in terms of the nondimensional coordinates.

$$k'^2 = 1 - \frac{4R}{X^2+(1+R)^2} \tag{23}$$

These coordinates are then expressed as functions of the variable S as given in Equations 15, 16, and 17. Then, the complementary modulus in Equation 23 can be written as

$$k'^2 = \frac{S^2}{4\left[1 + S \sin\beta + \frac{S^2}{4}\right]} \tag{24}$$

Since S has such a small magnitude, k'^2 can be expanded in the convergent binomial series

$$k'^2 = \frac{S^2}{4}\left\{1 - S\sin\beta + S^2\left[\sin^2\beta - \frac{1}{4}\right] + S^3\left[\frac{1}{2}\sin\beta - \sin^3\beta\right] + S^4\left[\frac{1}{16} - \frac{3}{4}\sin^2\beta + \sin^4\beta\right] + \ldots\right\} \tag{25}$$

In both elliptic integral expansions, 20 and 21, the term $\ln \frac{4}{k'}$ appears. This term may be expanded by the logarithmic series given in Reference (14).

$$\ln\left(\frac{4}{k'}\right) = \ln 8 - \frac{1}{2}\ln S^2 + \frac{1}{2}\ln\left[1 + S\sin\beta + \frac{S^2}{4}\right]$$

or

$$\ln\left(\frac{4}{k'}\right) = \ln 8 - \frac{1}{2}\ln S^2 + \left\{\frac{S}{2}\sin\beta + S^2\left[\frac{1}{8} - \frac{\sin^2\beta}{4}\right] + S^3\left[-\frac{\sin\beta}{8} + \frac{\sin^3}{6}\right] + S^4\left[-\frac{1}{64} + \frac{1}{8}\sin^2\beta - \frac{1}{8}\sin^4\beta\right] + \ldots\right\} \tag{26}$$

Equations 25 and 26 may now be used to express the elliptic integrals K and E as functions of the single variable S. After some algebraic manipulations, these equations become

$$K = \ln 8 - \frac{1}{2}\left[\ln S^2\right]\left[1 + \frac{S^2}{16} - \frac{S^3\sin\beta}{16}\right] + \frac{S\sin\beta}{2} + S^2\left[\frac{1}{8} - \frac{\sin^2\beta}{4} + \frac{\ln 8}{16}\right] - \left[\frac{S^2}{16}\right] + \cdots \tag{27}$$

and

$$E = 1 + S^2\left[\frac{\ln 8}{8} - \frac{1}{16}\right] + S^3\sin\beta\left[\frac{1}{8} - \frac{1}{8}\ln 8\right] - \frac{1}{2}\left[\ln S^2\right]\left[\frac{S^2}{8} - \frac{S^3\sin\beta}{8}\right] + \cdots \tag{28}$$

All variables in Equations 18 and 19 except δ have now been expressed as functions of S. As stated earlier, many frustum surfaces will be required to adequately approximate the double-curved surface of the nacelle. This requirement insures that the term S will be quite small. (A nominal value of 0.1 or less was chosen as a constraint.) The rapid convergence of such expansions as those of the elliptic integrals is dependent on this condition. The truncations of the infinite series formed by the multiplication of the terms in the integrands are also dependent on this size restriction of S. After performing the indicated operations and collecting

like terms, the velocity equations in truncated form may be written as

$$u = \int_{-S_1}^{S_1} \frac{\gamma}{4\pi} \left\{ \frac{2\sin\beta}{S} + \ln 8 - 1 + \sin^2\beta + S\left[\frac{5}{8}\sin\beta - \frac{1}{4}\sin\beta \ln 8 - \frac{1}{4}\sin^3\beta\right] + S^2\left[\frac{1}{4} - \frac{3}{16}\ln 8 + \frac{1}{4}\sin^2\beta \ln 8 - \frac{9}{16}\sin^2\beta + \frac{1}{8}\sin^4\beta\right] - \frac{\ln S^2}{2}\left[1 - \frac{S\sin\beta}{4} + S^2\left[-\frac{3}{16} + \frac{1}{4}\sin^2\beta\right]\right]\right\} ds \qquad (29)$$

and

$$v = \int_{-S_1}^{S_1} \frac{\gamma}{4\pi} \left\{ \frac{2\cos\beta}{S} + \sin\beta\cos\beta - S\left[-\frac{5}{8}\cos\beta + \frac{1}{4}\sin^2\beta\cos\beta + \frac{3}{4}\cos\beta \ln 8\right] - S^2\left[-\frac{1}{8}\sin^3\beta\cos\beta + \frac{11}{16}\sin\beta\cos\beta - \frac{3}{8}\ln 8 \sin\beta\cos\beta\right] - \frac{3}{8}\ln S^2\left[S\cos\beta - \frac{S^2\sin\beta\cos\beta}{2}\right]\right\} ds \qquad (30)$$

These equations may be integrated for a known vorticity distribution as a function of S, and as was suggested before, a simple linear distribution was chosen. The actual numerical values of γ are not known a priori, but the integration may be performed in terms of the unknown values γ_1 and γ_2 at $-S_1$ and S_1 and by expressing γ as a function of these constants and the variable S.

$$\gamma = \left[\frac{\gamma_2 - \gamma_1}{2 S_1}\right] S + \frac{\gamma_1 + \gamma_2}{2} \qquad (31)$$

The integrated velocity component equations now become

$$u = \frac{\gamma_2}{4\pi}\left\{ 2\sin\beta + S_1\left[\ln\frac{8}{S_1} + \sin^2\beta\right] + \frac{S_1^2}{3}\left[\frac{13}{24}\sin\beta - \frac{1}{4}\sin\beta\ln\frac{8}{S_1}\right.\right.$$

$$\left. - \frac{1}{4}\sin^2\beta\right] + \frac{S_1^3}{3}\left[\frac{3}{16} - \frac{3}{16}\ln\frac{8}{S_1} + \frac{1}{4}\sin^2\beta\ln\frac{8}{S_1}\right.$$

$$\left.\left. - \frac{23}{48}\sin^2\beta + \frac{1}{8}\sin^4\beta\right]\right\}$$

$$+ \frac{\gamma_1}{4\pi}\left\{ -2\sin\beta + S_1\left[\ln\frac{8}{S_1} + \sin^2\beta\right] - \frac{S_1^2}{3}\left[\frac{13}{24}\sin\beta - \frac{1}{4}\sin\beta\ln\frac{8}{S_1}\right.\right.$$

$$\left. - \frac{1}{4}\sin^2\beta\right] + \frac{S_1^3}{3}\left[\frac{3}{16} - \frac{3}{16}\ln\frac{8}{S_1} + \frac{1}{4}\sin^2\beta\ln\frac{8}{S_1}\right.$$

$$\left.\left. - \frac{23}{48}\sin^2\beta + \frac{1}{8}\sin^4\beta\right]\right\} \qquad (32)$$

$$v = \frac{\gamma_2}{4\pi}\left\{ 2\cos\beta + \sin\beta\cos\beta\, S_1 + \frac{S_1^2}{3}\left[\frac{3}{8}\cos\beta - \frac{\sin^2\beta}{4}\cos\beta\right.\right.$$

$$\left. - \frac{3}{4}\cos\beta\ln\frac{8}{S_1}\right] + \frac{S_1^3}{3}\left[\frac{\sin^3\beta\cos\beta}{8} - \frac{9}{16}\sin\beta\cos\beta + \frac{3}{8}\cos\beta\sin\beta\ln\frac{8}{S_1}\right]\Bigg\}$$

$$+ \frac{\gamma_1}{4\pi}\left\{ -2\cos\beta + \sin\beta\cos\beta\, S_1 - \frac{S_1^2}{3}\left[\frac{3}{8}\cos\beta - \frac{\sin^2\beta}{4}\cos\beta\right.\right.$$

$$\left. - \frac{3}{4}\cos\beta\ln\frac{8}{S_1}\right] + \frac{S_1^3}{3}\left[\frac{\sin^3\beta\cos\beta}{8} - \frac{9}{16}\sin\beta\cos\beta\right.$$

$$\left.\left. + \frac{3}{8}\cos\beta\sin\beta\ln\frac{8}{S_1}\right]\right\} \qquad (33)$$

As was pointed out earlier in this section, the first portion of the analysis does not include that contribution due to the local surface vortex strength that causes a discontinuous velocity through the frustum surface. The existence of the discontinuity in tangential velocity across a sheet of vorticity is illustrated in Appendix B. A more rigorous development for a very general case can be found in Reference (15). As shown by these two derivations, the magnitude of this discontinuity is equal to the local surface vortex strength γ.

As a verification of the velocity equations derived, the frustum shown in Figure 7 was used as a test case. At each of the numbered field points Equations 12 and 13 were numerically integrated. These results were extrapolated to yield the surface velocities on the inner and outer surfaces. These results were then expressed as the tangential and normal velocities to the surface and are shown in Figure 8. At the frustum midpoint the velocity equations 32 and 33 were evaluated and those results are also shown in Figure 8. From this figure one sees that within graphical accuracy the field point equations yield a continuous normal velocity component through the sheet of vorticity and a discontinuous tangential component. The magnitude of this discontinuity is equal to γ. One also sees that the singular equations yield the same value for the normal velocity component as the limiting or extrapolated values of the outer and inner field solutions and the tangential component is equal to the average of the inner and outer field point solutions.

From this observation it can be seen that it will be necessary to add or subtract the quantity $\frac{\gamma}{2}$ to the tangential velocity obtained by the

singular point solution depending on whether the inner or outer surface value is desired.

NUMERICAL SOLUTION

After the given nacelle surface has been approximated by many frustum surfaces, the numerical solution consists of finding the γ distribution that will cause the freestream flow to move tangentially to the frustum midpoints. Once this distribution is known, the resulting velocity components at any point may be found, and from these, the resulting pressure field about the body can be determined.

To illustrate the steps involved, an annular torus in a uniform flow will be used as an example. The torus surface is first broken into ten frustum surfaces as shown in Figure 3. The midpoints of the frustums and their intersections or corners have been numbered to clarify the discussion. The problem consists of finding the velocity at the even numbered midpoints, point 2 for example, due to the effect of all the frustums of vorticity.

The first frustum to be examined is frustum 1-3 for which the point 2 is a singular point. The singular point velocity equations are easily programmed for the digital computer and the resulting equations, including the $\frac{\gamma}{2}$ term, may be written as functions of the corner γ values.

$$u_{21} = M_{21}\,\gamma_3 + M'_{21}\,\gamma_1 \tag{34}$$

$$v_{21} = N_{21}\,\gamma_3 + N'_{21}\,\gamma_1 \tag{35}$$

In the double subscripting used in these two equations, the first number refers to the point at which the velocity is desired. The second number refers to which one of the ten frustums influencing the point is presently being considered.

For the remaining nine frustums, point 2 is a field point and Equations 12 and 13 may be used to express the influence of each frustum on point 2 in terms of the corner δ values for that particular frustum. The numerical evaluation of these integrals was accomplished by using Gaussian quadrature formulas explained in Reference (16).

These formulas have been programmed for the digital computer and can be found in most program libraries. Briefly, this method of integral evaluation consists of first evaluating the integrand at several specified points in the interval of integration. These values are then substituted into the algebraic formulas and are multiplied by weighting factors. The particular quadrature formula chosen will dictate the number of points and their location. In order to save computer time and insure an accurate integration, four quadrature subroutines were used. A 2-point Gaussian quadrature, which integrates polynomials up to degree 3 exactly, was used when the frustum surface length was small and the field point was not close to the frustum. A 10-point Gaussian quadrature, which integrates polynomials up to degree 19 exactly, was used when the frustum surface was large and the field point close to that frustum. The 4-point and 6-point formulas were used on intermediate cases. The test parameter used to determine which subroutine would be chosen in a given case was a ratio of the distance from the frustum midpoint to the field point divided by the frustum surface length. Many combinations of field point positions and frustum sizes were examined. In each case the integration was done by a 2-point, a 4-point, a 6-point, and a 10-point Gaussian quadrature subroutine. It was found that for ratios greater than 20, a 2-point quadrature formula was sufficient for single

precision accuracy. In the range of ratio values from 4 to 20, a 4-point formula was used. If the ratio was in the range of 1.5 to 4, a 6-point formula gave the necessary accuracy, and for ratios less than 1.5 the 10-point formula was used.

After the field equations for the nine frustums have been integrated, the velocity component equations at point 2 can then be written as two linear algebraic equations in terms of all the corner values of δ and their geometry dependent coefficients.

$$u_2 = \sum_{n=1}^{11} [cogu]_{2n-1} \delta_{2n-1} \tag{36}$$

$$v_2 = \sum_{n=1}^{11} [cogv]_{2n-1} \delta_{2n-1} \tag{37}$$

The coefficients of the individual δ terms are merely the sums of the coefficients of like δ terms determined in the singular point and field point integrations.

The boundary condition at point 2 may now be written in terms of the eleven corner values of δ. If the fluid is to flow tangentially to the surface, the ratio of radial component of velocity to the total axial component must be equal to the slope of the frustum surface. This may be written mathematically as

$$\frac{v_2}{V_\infty + u_2} = \tan\beta_2 \tag{38}$$

or

$$v_2 - u_2 \tan\beta_2 = V_\infty \tan\beta_2 \tag{39}$$

Equation 39 can be simplified by adding the coefficients of like γ terms to form a single equation expressing the tangential flow requirement at point 2 in terms of the unknown corner γ values.

$$\sum_{n=1}^{11} Q_{2n-1} \gamma_{2n-1} = V_\infty \tan\beta_2 \tag{40}$$

In the point 2 example there are eleven unknown values of γ. This same procedure as outlined above may be repeated for the nine remaining frustum midpoints yielding a matrix of ten linear algebraic equations in eleven unknowns. An additional equation is required for a solution.

The torus was chosen as an example because it would allow a comparison to be made with a simple analytic solution, that of the two-dimensional cylinder. For simplicity it was assumed that the cylinder had no circulation about its cross section. Therefore, to make a comparison the circulation about the torus cross section was also restricted to a value of zero. Mathematically, this requirement introduces no new unknowns and yields the eleventh equation needed for a solution. This equation may be written as

$$\oint \gamma \, ds = 0$$

For a known nacelle geometry and a linear vorticity function of S, the above equation can be integrated and expressed as an algebraic equation in terms of the corner values of γ.

$$\sum_{n=1}^{11} \text{cogs}_{2n-1} (\gamma)_{2n-1} = 0 \tag{41}$$

With the additional boundary condition, Equation 41, the number of independent equations now equals the number of unknowns. These eleven simultaneous, linear, algebraic equations in eleven unknowns can be stored in matrix form within the computer. The inversion of the coefficient matrix and consequently the solution for the δ matrix was found by means of a standard Fortran subroutine. By using these δ values the velocity components at point 2 due to the nacelle of vorticity may be found from Equations 36 and 37.

The velocity field has now been determined by simply satisfying the kinematic equation 1. To obtain the pressure distribution, a dynamic relationship involving the speed and pressure will be needed. Under the flow restrictions used, the incompressible form of Bernoulli's equation is sufficient.

$$p + \frac{1}{2}\rho V^2 = \text{constant} \tag{42}$$

In order to make the pressure variation independent of the freestream conditions, the dimensionless pressure coefficient is introduced.

$$C_p = \frac{p - p_\infty}{\frac{1}{2}\rho_\infty V_\infty^2} \tag{43}$$

This can be simplified by using Bernoulli's equation to obtain the form

$$C_p = 1 - \left[\frac{V}{V_\infty}\right]^2 \tag{44}$$

This equation was programmed so that the pressure coefficient was then computed at each frustum point.

The corner coordinates of the frustums are used as inputs to the computer program developed. The 10-frustum torus example had a run time on the IBM 360-65 of 15 seconds. A dimensionless freestream velocity of 100 was used for this example. The resulting surface vorticity distribution is shown in Figure 4. Note that the vorticity distribution is a continuous function of the surface length and is linear on each frustum. The velocity at each midpoint due to the uniform flow with the superimposed velocities caused by the nacelle of vorticity is shown in Figure 9. From this figure one sees that the requirement of tangential flow at the surface is met.

The pressure distribution about the torus is illustrated in Figure 10 by plotting C_p as a function of the axial length. A comparison of the three-dimensional torus with the two-dimensional cylinder can then be made. By using an annular torus with a large radial length to the circular torus centerline (a value of 10) and a small radius for the actual circular cross section (a value of 1) it was felt that the program could be verified by a comparison to the known cylindrical pressure distribution found in references such as (10). A close correlation is found to exist which gives credibility to the program.

For cowls of finite length the restriction of zero circulation about the cross section is not recommended. A modified Kutta condition is proposed that requires a trial-and-error method of guessing the proper slope of the streamline as it leaves the trailing edge. For two-dimensional wing programs a common boundary condition is to require the slope to be the average between the upper and lower wing slopes at the trailing edge. As a first approximation, this same condition was used to supply the additional equation necessary to have the same number of unknown γ values as independent

equations. The program is run and the pressure coefficients on the inner and outer surfaces at the trailing edge are compared. If they are not the same, an iteration must be performed by changing the assumed streamline slope until the two pressures match. This scheme does not strongly affect the forward pressures, but sufficient experimental data was not available to thoroughly check the adequacy of the procedure.

A different boundary condition that is used to replace the modified Kutta condition described above is discussed in the next section. In this iteration scheme the matching parameter is not the two pressures at the trailing edge but rather the mass flow through an experimental nacelle.

RESULTS AND CONCLUSIONS

A literature search for experimental data to check the validity of the program was not very productive. In early experimental testing it was found that for long nacelles the aft shape did not materially affect the forward pressure distribution. It was also discovered that one of the most significant parameters affecting changes in the pressure distribution about the surface was the mass flow passing through the nacelle. This flux is usually measured by the velocity ratio, $\frac{V_I}{V_\infty}$, where V_I is the average axial velocity at the inlet. These two test results led experimenters to build long nacelles with bulky supports and controls at the aft portion of the nacelle. The experimenters controlled the mass flow by extraneous devices such as a movable plug in the rear section. This type of construction limited the use of the data obtained for checking the computer program since the Kutta condition was not realistically met in these experiments.

Another variation in experimental procedure from conditions imposed in the programmed problems is that the freestream Mach number for the tests were usually large enough to introduce compressibility effects.

A third difference found in many experiments was the use of a large center body or hub used as a spinner for a propeller or fan and as a support mechanism for the nacelle.

After a lengthy examination of data available, it was decided to use the NACA data in Reference (1) since it was the most complete and thorough. The NACA 1-60-050 was chosen as a "model" for comparison with the nacelle program. The NACA tests used a long cylindrical midsection onto which different nose sections could be attached. The experimenters were only

interested in the forward pressure on the outer surface of this nacelle and had many extraneous control devices and supports in the aft section. These mechanisms were assumed to be far enough downstream so that they would not affect the nose section flow. The nacelle shape used to define input coordinates for the computer program is shown in Figure 11. It has an NACA 1-60-050 nose section followed by a long, uniform midsection. The aft section shape is not the same as that of the NACA test setup. It was assumed that the long midsection would place the rear section far enough away from the nose that this inaccuracy in shape description would be of secondary importance in influencing the nose pressures when compared with the mass flow effects.

In the experimental testing a freestream Mach number of 0.4 was used which would give rise to some compressibility effects. To account for this in the program, a Gothert rule correction as outlined in Reference (18) was incorporated into the program. For subsonic flow this requires the shrinking of the radial coordinates by the factor $(1-M_\infty^2)^{\frac{1}{2}}$. The problem is then solved for incompressible flow using this affinely related nacelle and the resulting pressure coefficients are divided by the term $(1-M_\infty^2)$. These new pressure coefficients are the values expected on the original body with a freestream Mach number of M_∞. Since the experimental Mach number was not too high, it was felt that this correction would be adequate and would allow a fair comparison of results.

The NACA tests were run at several different velocity ratios which were attained through the use of an external plug at the aft end of the long nacelle. In order to determine at what velocity ratio the computer nacelle was operating, a special subroutine was written. The average axial

velocity at the inlet can be found by an integration of the axial inlet velocity with respect to the differential area and dividing this integral by the inlet area.

$$V_I = \frac{\int_0^{R_{inlet}} (u_{inlet}\, 2\pi r)\, dr}{\pi (R_{inlet})^2}$$

This integration can be performed graphically if the inlet velocities at several radial distances are known. To find velocities in the field about the nacelle, another subroutine was written. The use of this subroutine occurs after the vorticity of the entire nacelle surface is found. The points at which the velocity is desired are treated as field points just as in the vorticity solution. Equations 12 and 13 are integrated by the Gaussian quadrature subroutines and since the corner δ's are known, the velocity components due to each frustum can be found directly.

Since the original tests did not satisfy a true Kutta condition, the nacelle program criterion of a pressure matching on the inner and outer surfaces at the trailing edge was discarded for this example. In its place a trial streamline slope was chosen near the trailing edge and the resulting velocity ratio was compared to that of the NACA test. An iteration of slopes was performed until the nacelle program velocity ratio closely matched that of the NACA.

In the examples to be given a 40-frustum nacelle was used to approximate the shape illustrated in Figure 11. A high density of frustums were used in the nose region where the radius of curvature was small and greater

accuracy was desired. The inputs required by the program were easy to prepare, requiring only a good definition of the nacelle in order to read the corner coordinates of the frustums. Three trials were usually sufficient to match the velocity ratios of the NACA tests, and each computer run took less than one minute on the IBM 360-65.

Two NACA velocity ratios were chosen for comparison with the nacelle program. The first pressure comparison shown in Figure 12 is for a nacelle program velocity ratio of 0.16 and an NACA velocity ratio of 0.13. The second comparison shown in Figure 13 is for a nacelle program value of 0.61 and an NACA value of 0.67.

In both of these examples the pressure coefficients from the experimental test and the computer program were sufficiently close to illustrate the usefulness of the program in predicting the pressure distribution about a nacelle. The shape of the computer pressure curve follows the variation in the experimental test points quite closely in spite of differences between the two cases. These differences include such factors as aft end geometry, method of mass flow control, angle of attack variations, and the method used by the computer to extrapolate the incompressible values to compressible ones. The ease with which the pressure distribution about a nacelle can be obtained from this program should make it a valuable tool in nacelle analysis.

RECOMMENDATIONS FOR FURTHER STUDY

Probably the most important continuation of this work would be in the area of experimental verification of the program with emphasis being placed on establishing a reliable Kutta condition. This would probably require an extensive experimental program of nacelle testing to determine an empirically derived condition to be met at the trailing edge.

Several additions could be made to the present program to increase its usefulness. It would be desirable to have the option of including a center body within the nacelle. One way this could be accomplished is by locating a series of sources and sinks of unknown strength on the axis. A similar number of points on the center body surface would then be chosen as additional field points at which a tangential flow must occur. The analysis would then consist of requiring tangential flow at frustum midpoints and center body field points due to the vorticity surface, the collection of sources and sinks, and the freestream velocity. The number of equations and unknowns has been increased by the number of sources and sinks involved. After the matrix of coefficients has been inverted, the corner δ values and the strengths of the sources and sinks could be determined. The program would then proceed just as in the present case with the addition of the source and sink contributions.

A number of improvements might be made by applying results from viscous flow theory. A source ring could be located within the nacelle and an "open" nacelle could be examined. That is, the inner and outer surfaces would not meet at the trailing edge but would extend back indefinitely and would be separated by the small volume of flow due to the source ring.

This thin annular cylinder would approximate the boundary layer shed by an actual nacelle. This system might lead to a more realistic trailing edge flow.

As is often the case in a viscous analysis, a nonviscous solution is first required as a starting condition. The present program would provide that solution and might allow a viscous subroutine to be included as an option in an expanded program.

LITERATURE CITED

1. Baals, D. D. and Smith, N. F. The development and application of high-critical-speed nose inlets. United States National Advisory Committee for Aeronautics Report 920. 1948.

2. Nichols, M. R. and Keith, A. L., Jr. Investigations of a systematic group of NACA 1-series cowlings with and without spinners. United States National Advisory Committee for Aeronautics Technical Note 950. 1949.

3. Pendley, R. E. and Robinson, H. L. An investigation of several NACA 1-series nose inlets with and without protruding central bodies at high-subsonic Mach numbers and at a Mach number of 1.2. United States National Advisory Committee for Aeronautics Technical Note 3436. 1955.

4. Hink, G. R. Axisymmetric nacelle potential flow program. Renton, Washington, The Boeing Company (document) D6-17420. circa 1964.

5. Smith, A. M. O. and Pierce, J. Exact solution of the Neumann problem. Calculation of the noncirculatory plane and axially symmetric flows about or within arbitrary boundaries. Long Beach, California, Douglas Aircraft Company Report ES26988. 1958.

6. Emmons, N. W. The numerical solution of compressible flow problems. United States National Advisory Committee for Aeronautics Technical Note 832. 1944.

7. Southwell, R. V. Relaxation methods in engineering science. Oxford, England, Clarendon Press. 1940.

8. Colehour, J. L. and Gilbert, R. A relaxation solution for two-dimensional and axisymmetric potential flow problems. Renton, Washington, The Boeing Company (document) D6-18087 TN. 1966.

9. Tripodi, R. Analytical investigations of inlet cowls. Renton, Washington, The Boeing Company (document) D6-11245 TN. 1967.

10. Kuethe, A. M. and Schetzer, J. D. Foundations of Aerodynamics. 2nd ed. New York, N. Y., John Wiley and Sons, Inc. c1959.

11. Karamcheti, K. Principles of ideal-fluid aerodynamics. New York, N. Y., John Wiley and Sons, Inc. c1966.

12. Kuchemann, D. and Weber, J. Aerodynamics of propulsion. 1st ed. New York, N. Y., McGraw-Hill Book Co., Inc. 1953.

13. Jahnke, E. and Emde, F. Tables of functions. 4th ed. New York, N. Y., Dover Publication, Inc. c1945.

14. Burington, R. S. Handbook of mathematical tables and formulas. 3rd ed. Sandusky, Ohio, Handbook Publishers, Inc. 1956.

15. Kellogg, O. D. Foundations of potential theory. Berlin, Germany, Verlag Von Julius Springer. 1929.

16. Krylov, V. J. Approximate calculation of integrals. New York, N. Y., Macmillan. 1962.

17. Yuan, S. W. Foundations of fluid mechanics. Englewood Cliffs, N. J., Prentice-Hall, Inc. c1967.

18. Liepmann, N. W. and Roshko, A. Elements of gasdynamics. New York, N. Y., John Wiley and Sons, Inc. c1957.

ACKNOWLEDGEMENTS

The author wishes to express his gratitude do Dr. J. D. Iversen for his guidance and assistance in completing this thesis; to Dr. E. W. Anderson for his helpful suggestions in preparing the manuscript; to the Boeing Company for providing the initial opportunity to work on this project; and to my wife, Wanda, for typing the manuscript.

APPENDIX A: FIGURES

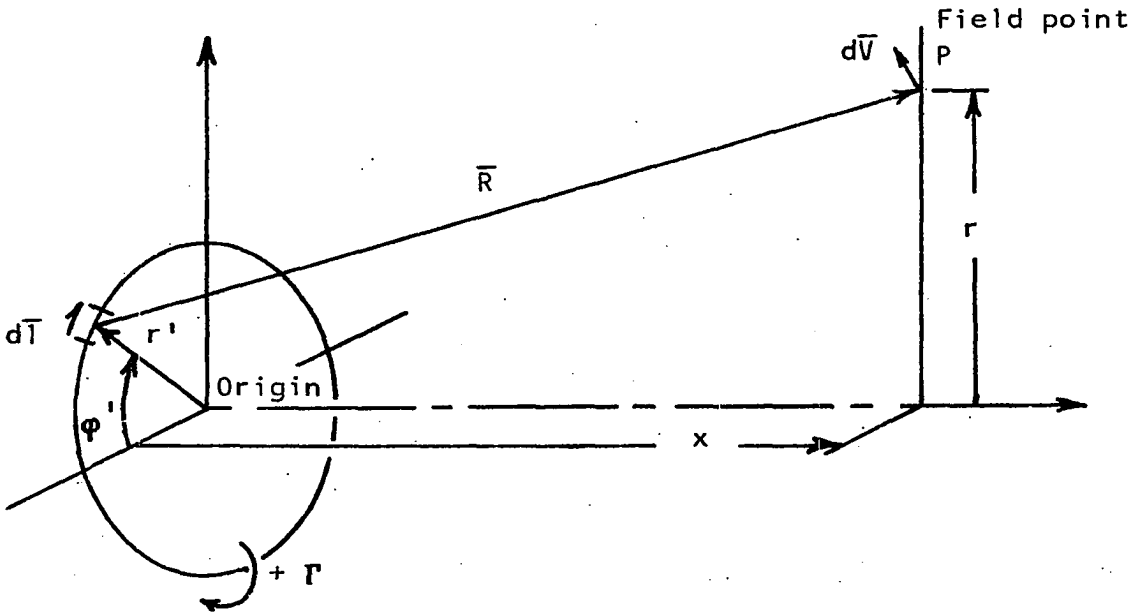

Figure 1. A vortex ring and field point

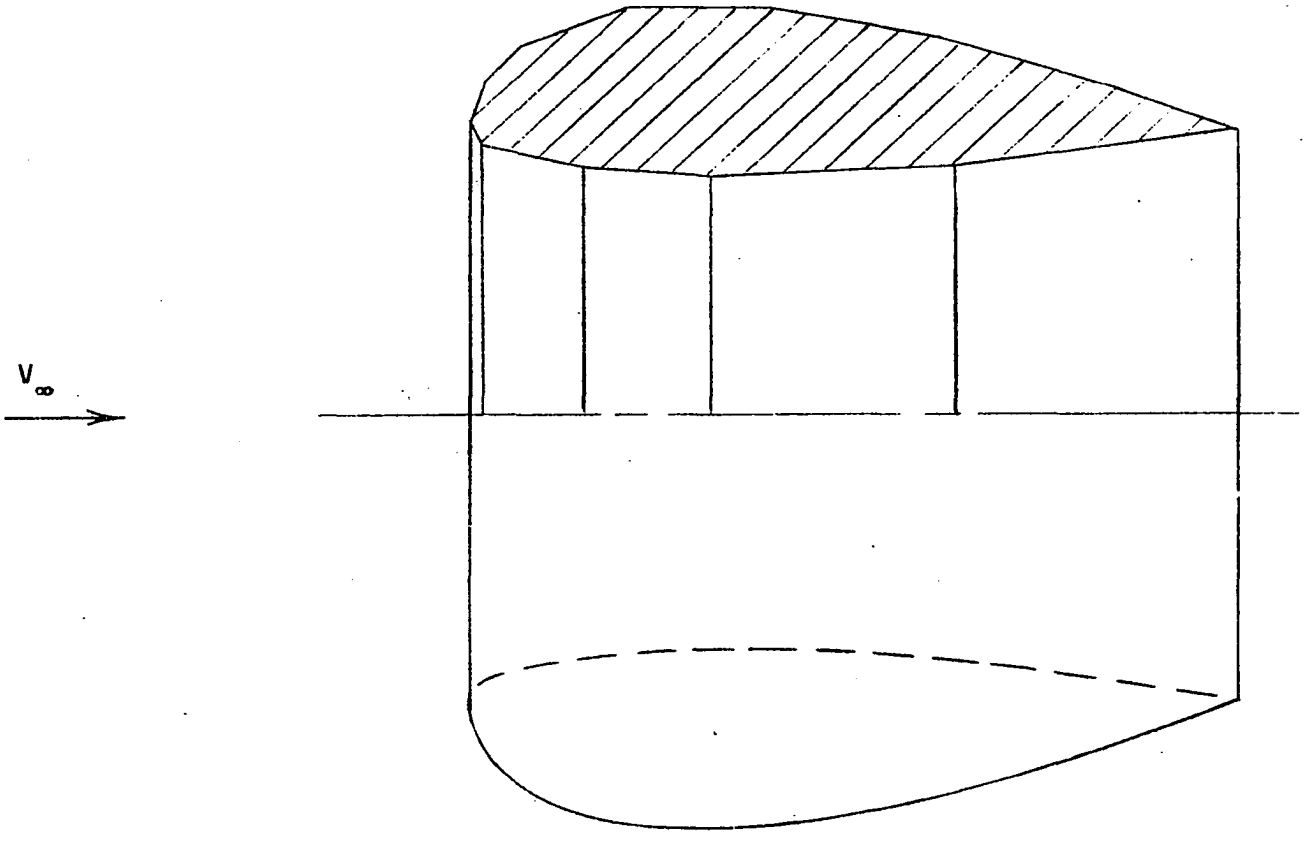

Figure 2. The replacement of the actual double-curved nacelle surface shown by a half section

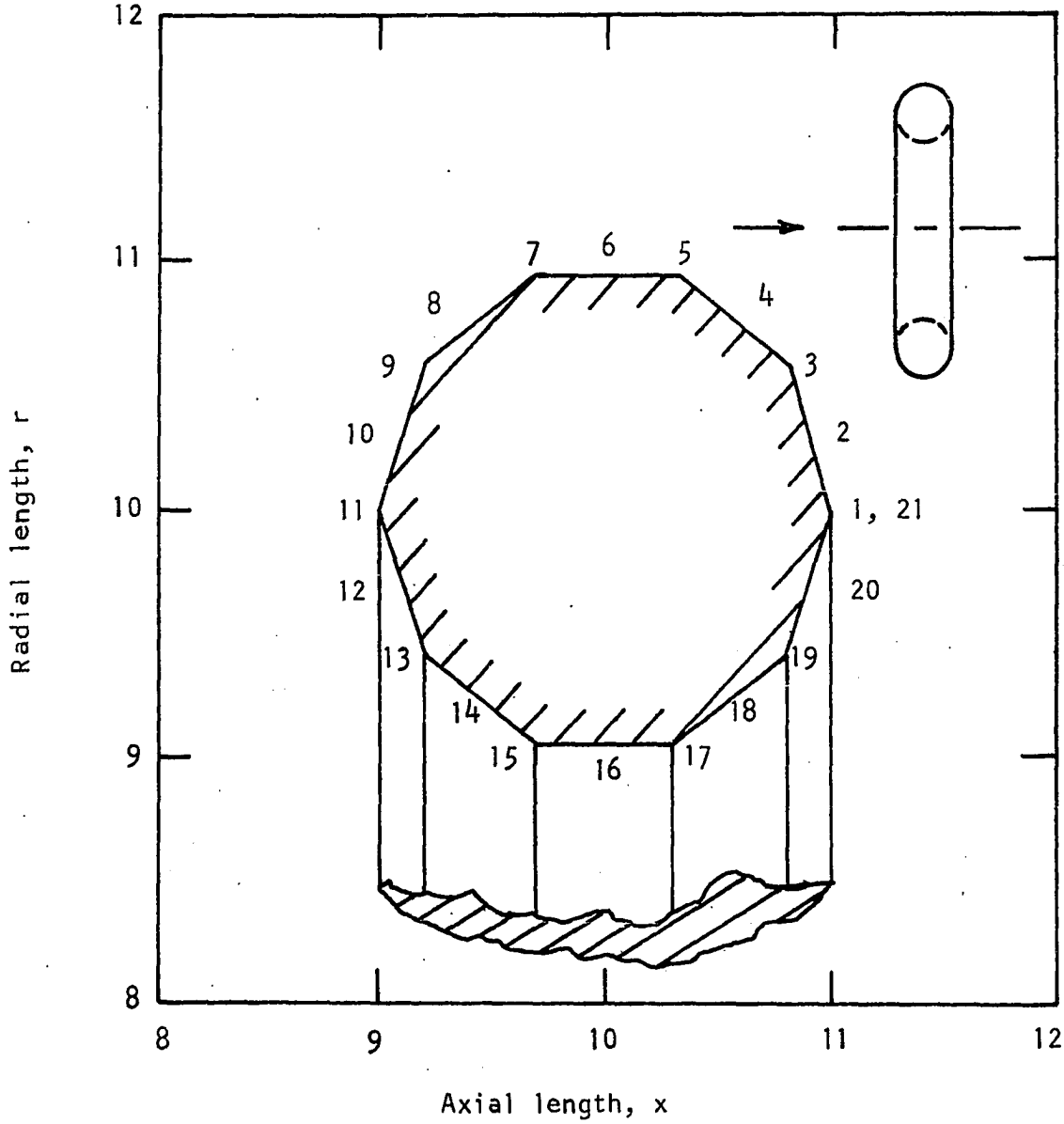

Figure 3. An annular torus with a frustum surface approximation

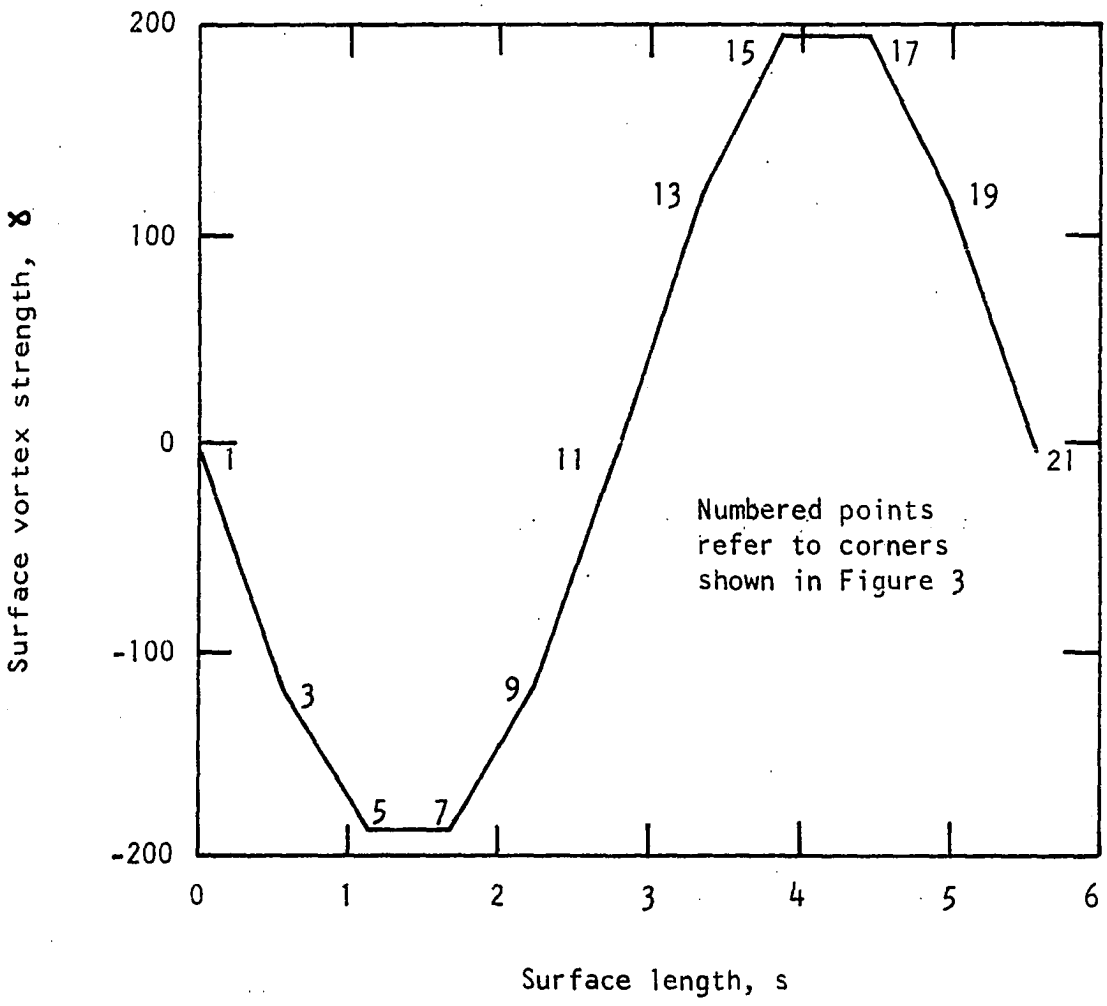

Figure 4. Surface vortex strength as a function of surface length for the 10-frustum torus shown in Figure 3

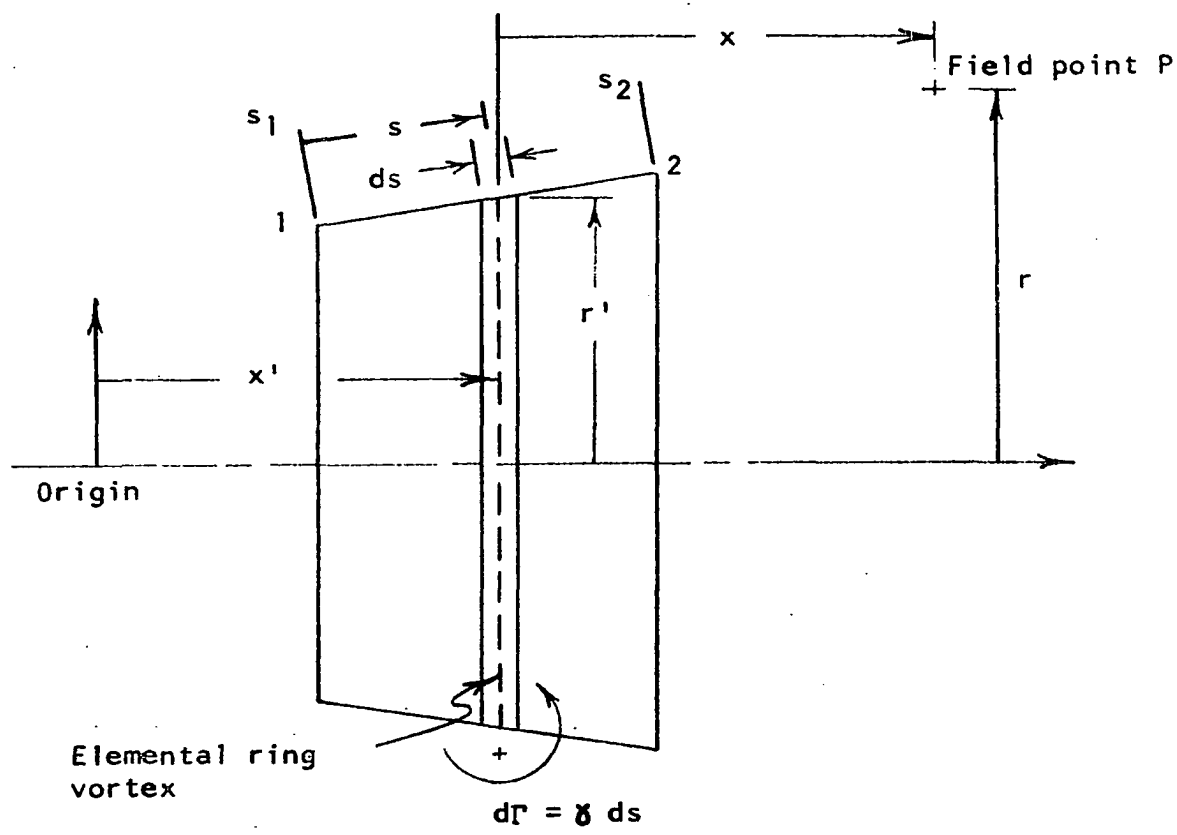

Figure 5. Coordinate system used when considering the effects of a single frustum at a field point

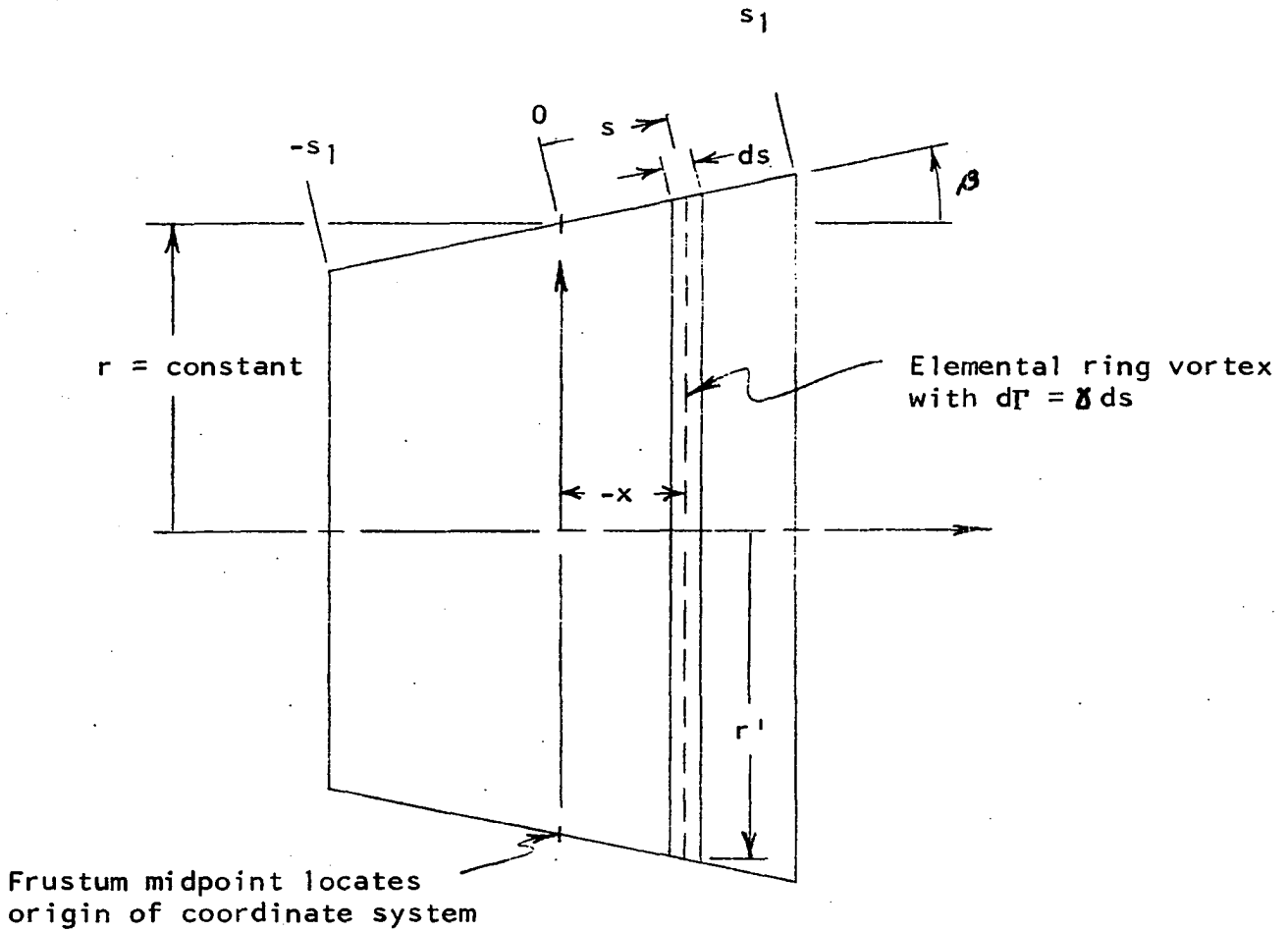

Figure 6. Coordinate system used when considering the effect of a single frustum on its own midpoint

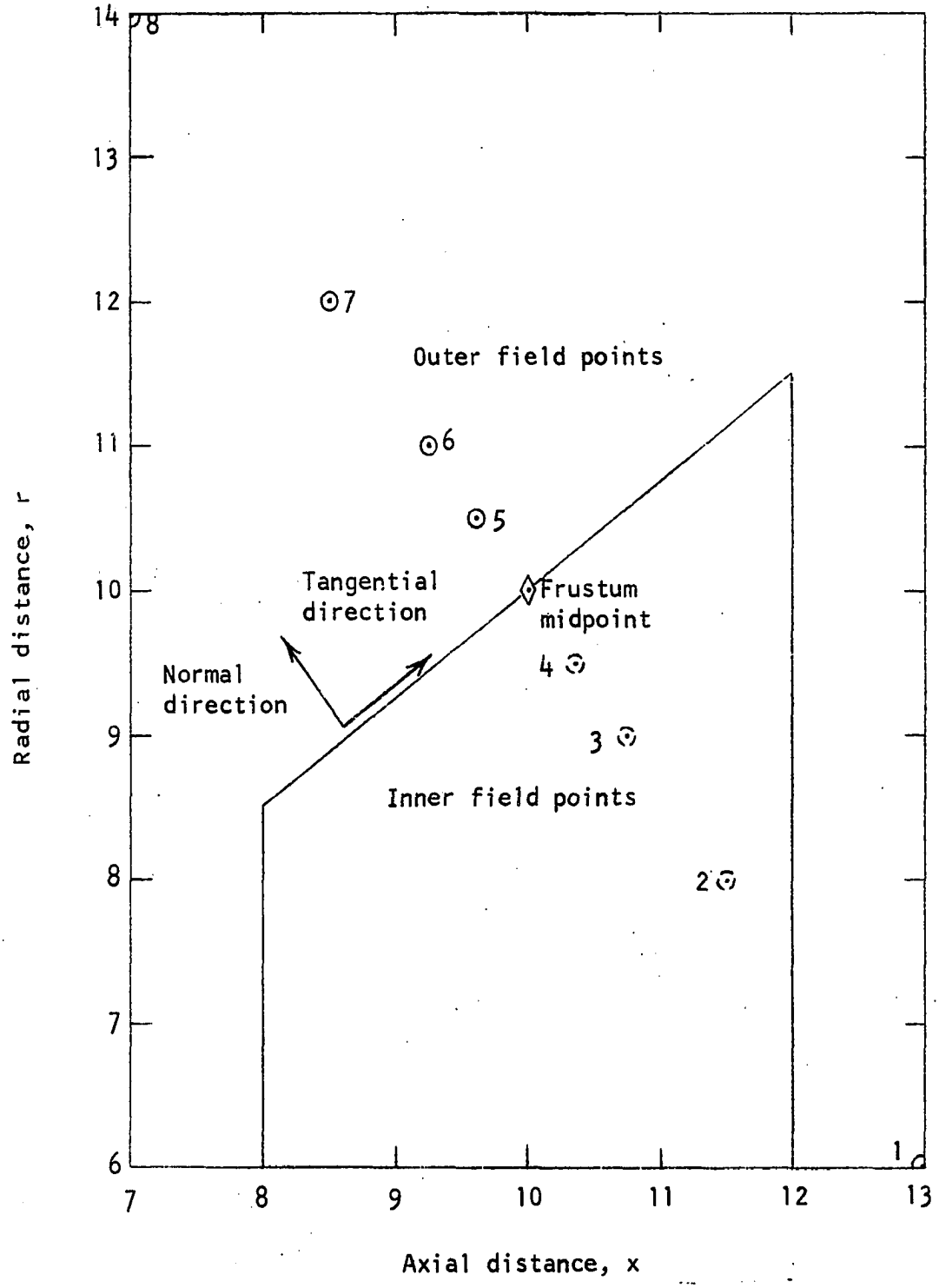

Figure 7. Frustum used as test case to check velocity equations

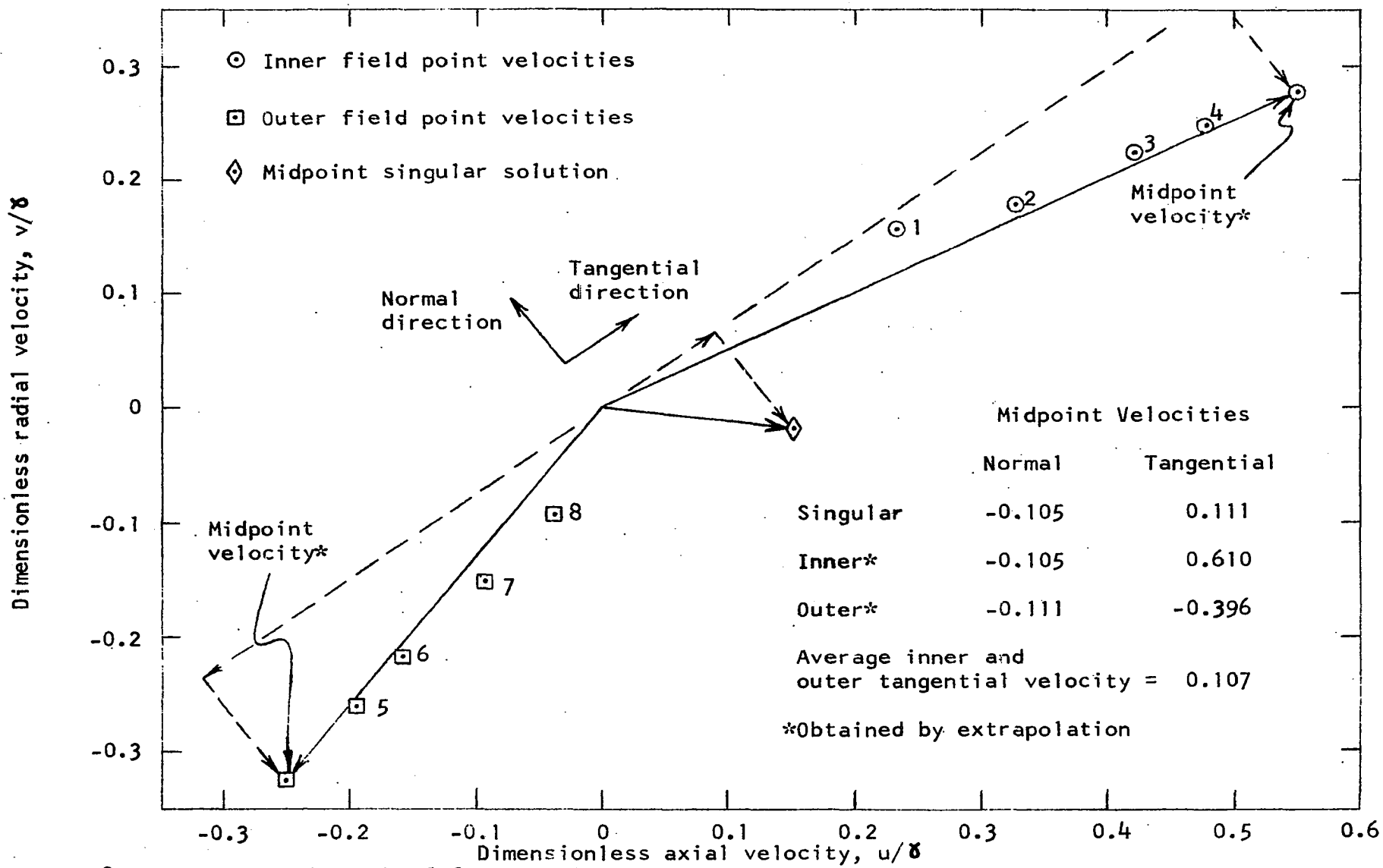

Figure 8. Velocity hodograph of frustum with constant δ

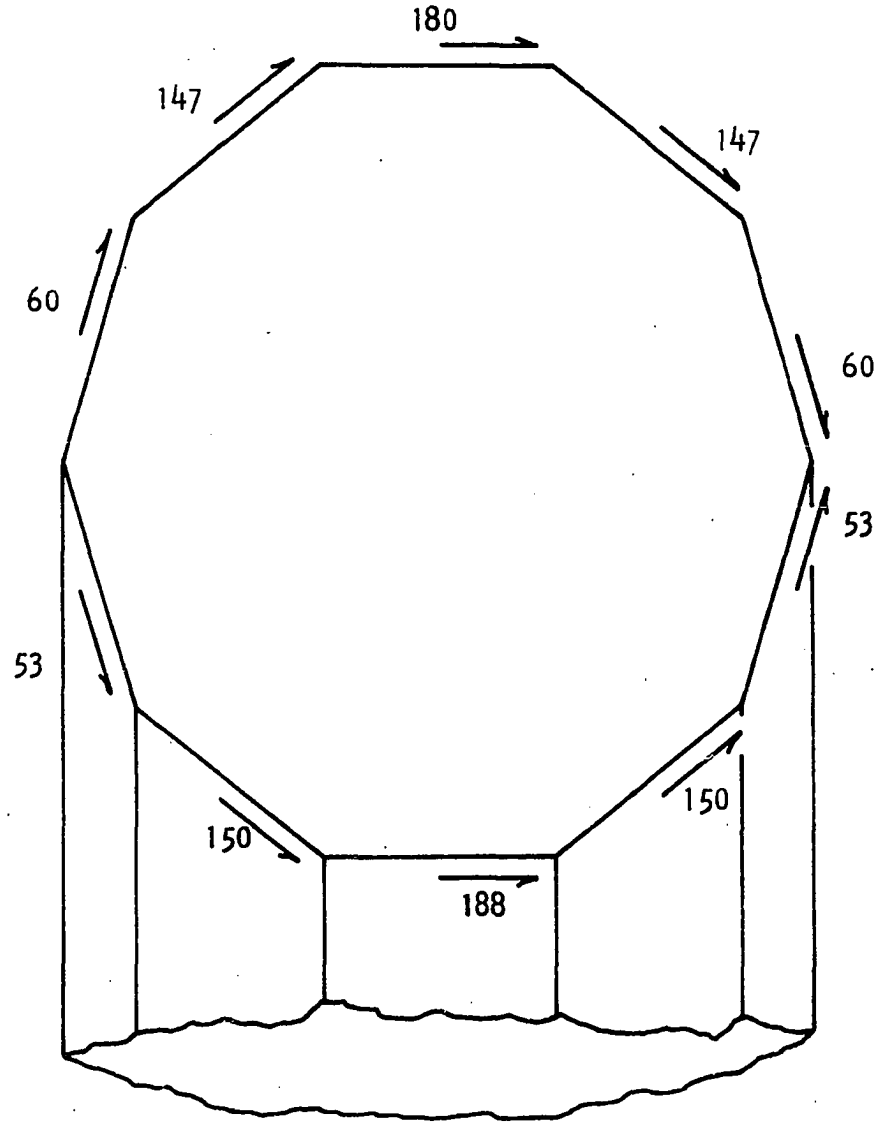

Figure 9. Midpoint velocities on torus of Figure 3 with freestream velocity of 100

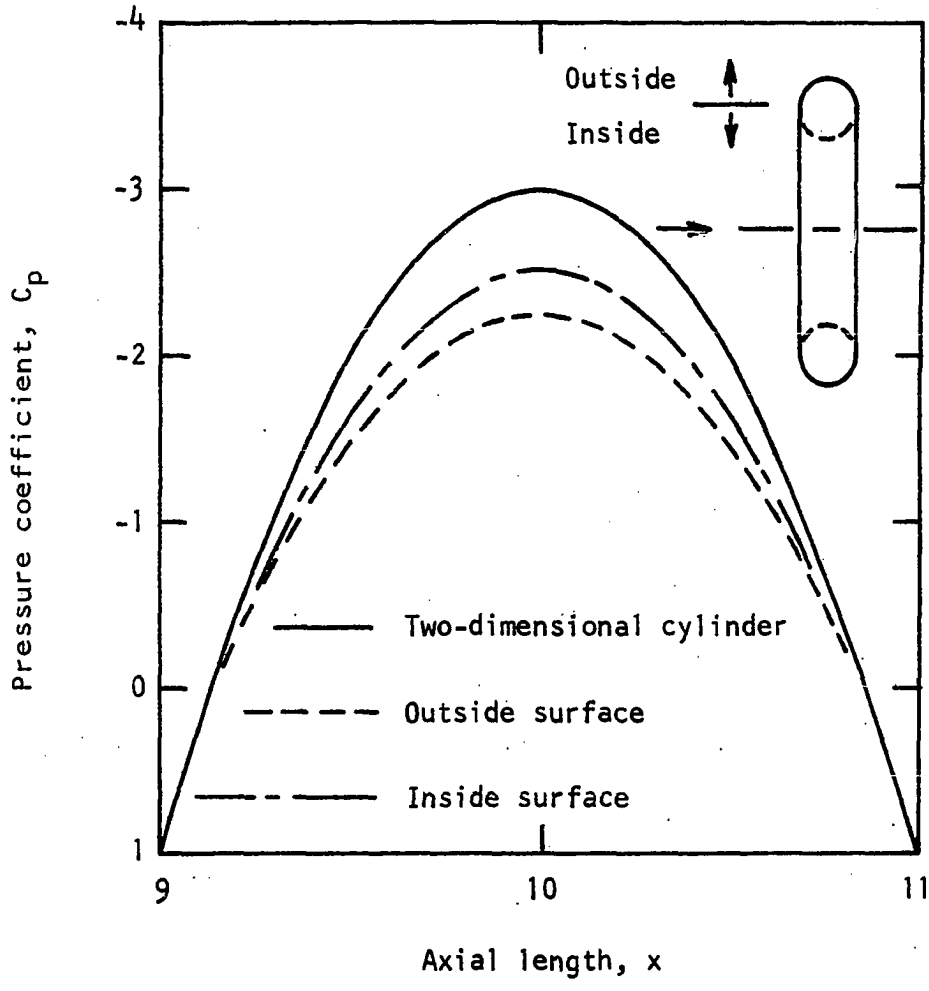

Figure 10. Pressure distribution comparison between a cylinder and the torus shown in Figure 3

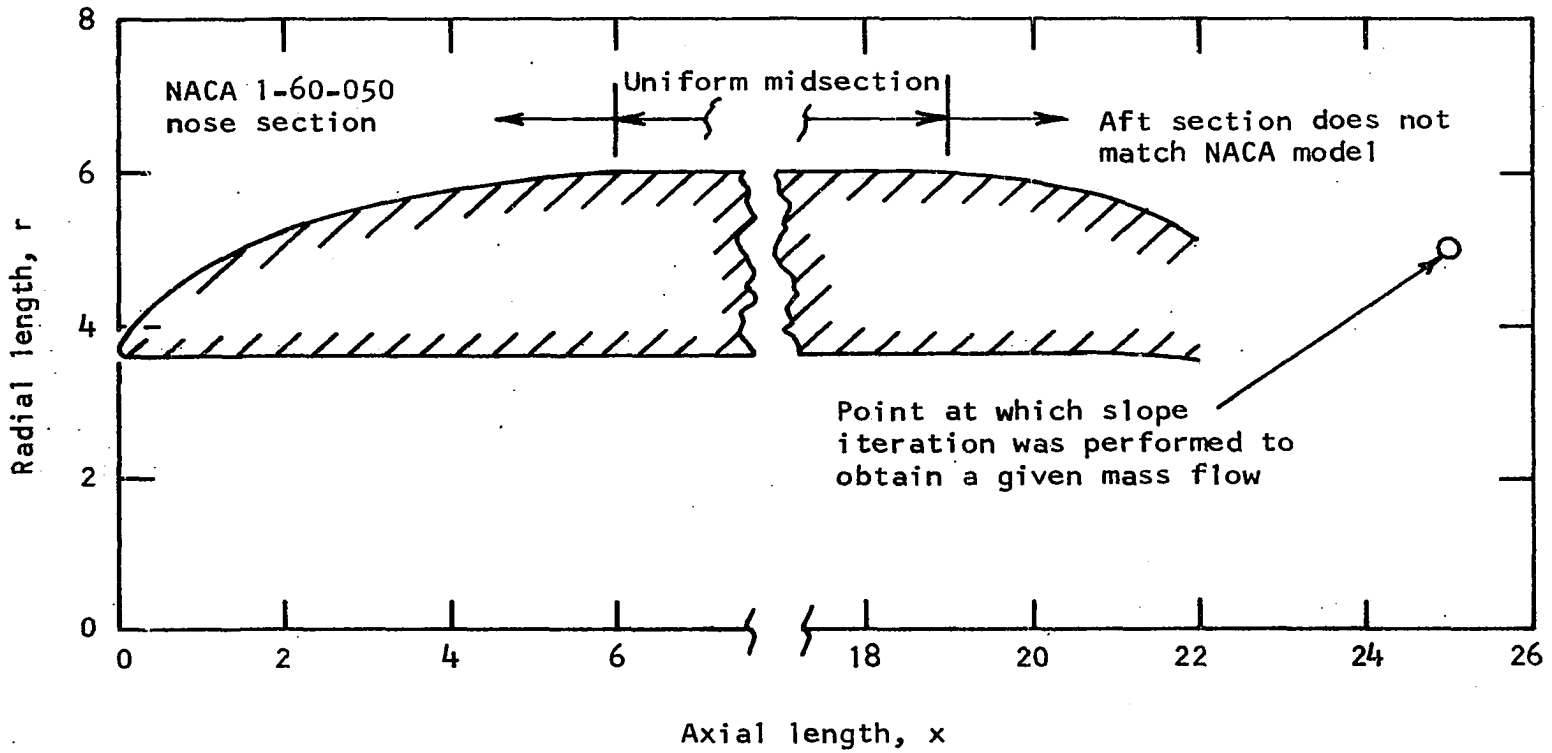

Figure 11. Cross section of nacelle with NACA 1-60-050 nose section

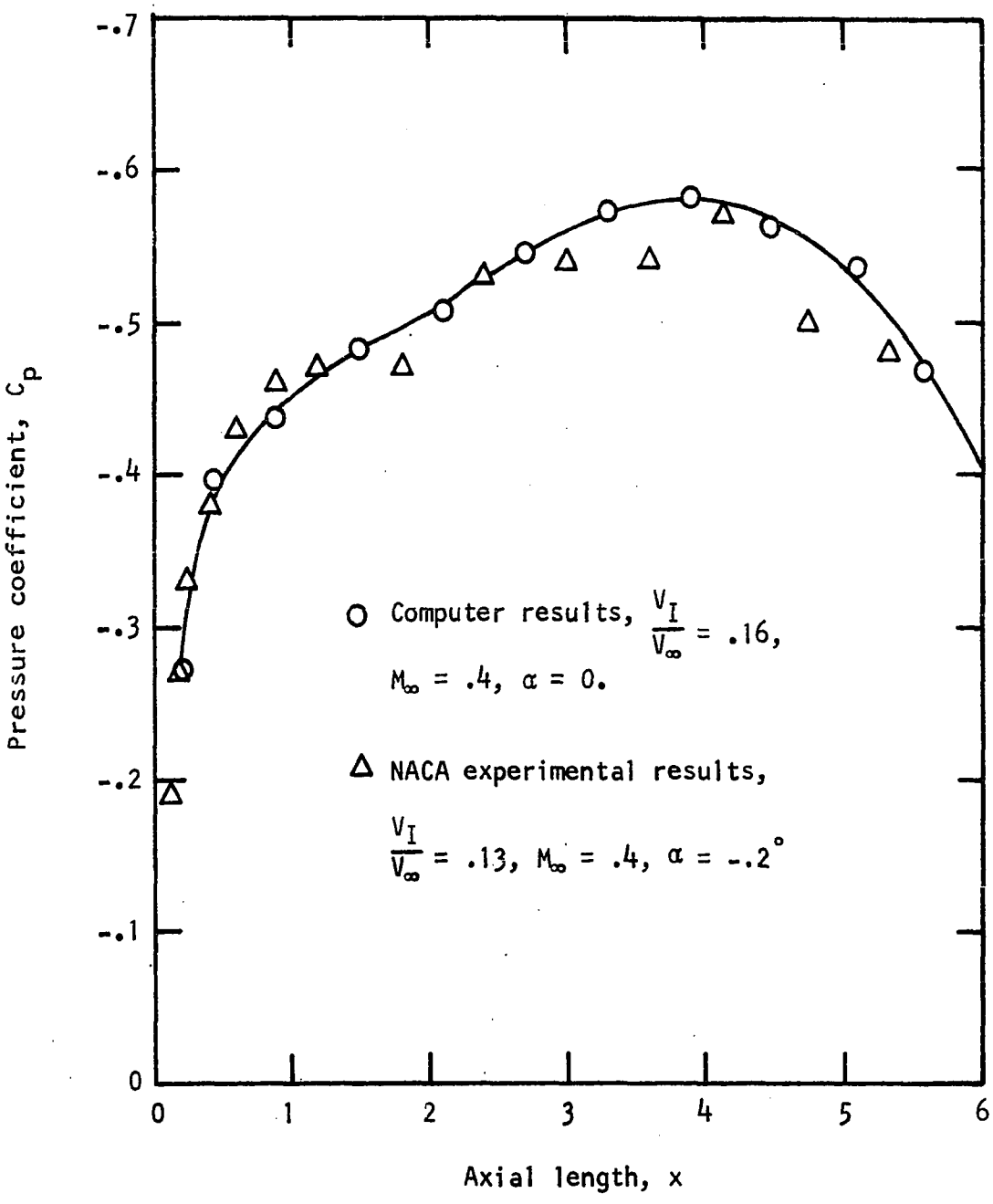

Figure 12. Pressure distribution on the external surface of an NACA 1-60-050 nacelle section with a low mass flow

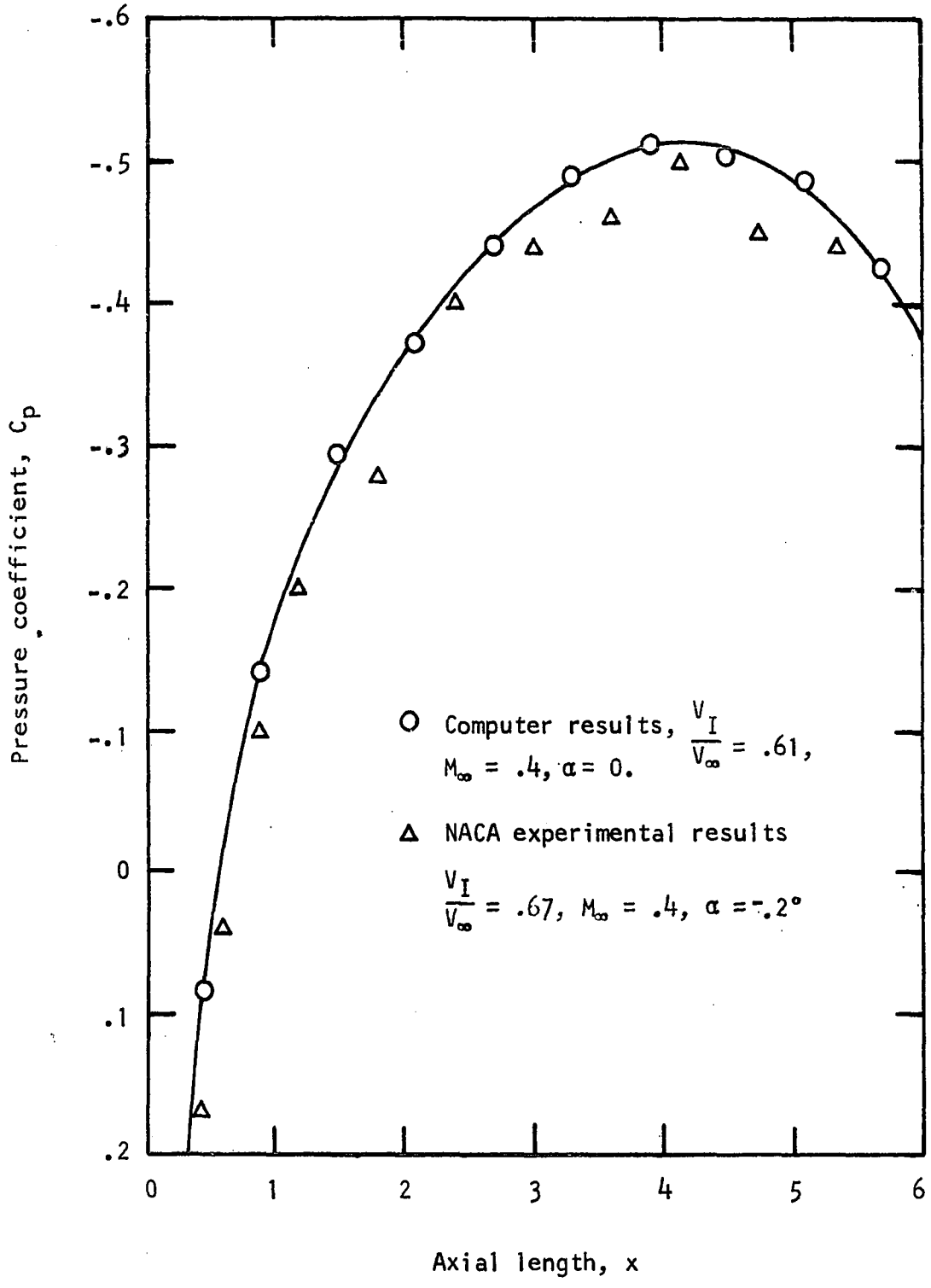

Figure 13. Pressure distribution on the external surface of an NACA 1-60-050 nacelle section with a high mass flow

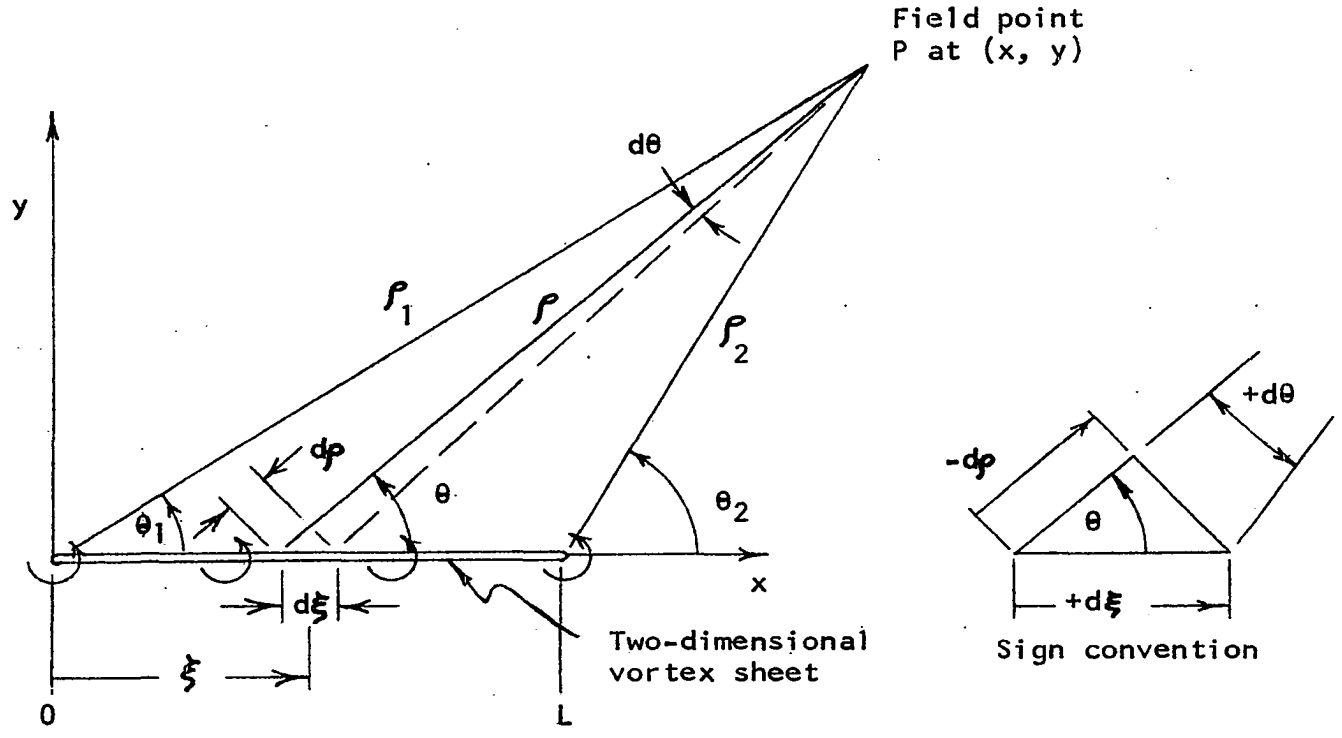

Figure 14. Two-dimensional vortex sheet

APPENDIX B: DISCONTINUITY OF VELOCITY ACROSS A SHEET OF VORTICITY

To simplify the illustration, a flat sheet of constant vorticity extending from x = 0 to x = L as shown in Figure 14 will be examined. The velocity component equations at the field point P are given in Reference 11.

$$u = \frac{-\gamma}{2\pi} \int_0^L \frac{y}{(x-\xi)^2 + y^2} \, d\xi \tag{45}$$

$$v = \frac{\gamma}{2\pi} \int_0^L \frac{x - \xi}{(x-\xi)^2 + y^2} \, d\xi \tag{46}$$

One sees from the same illustration that these may also be written as

$$u = \frac{-\gamma}{2\pi} \int_0^L \frac{\sin\theta}{\rho'} \, d\xi \tag{47}$$

$$v = \frac{\gamma}{2\pi} \int_0^L \frac{\cos\theta}{\rho'} \, d\xi \tag{48}$$

From the geometry in Figure 14 the equations

$$d\theta = \frac{\sin\theta \, d\xi}{\rho'} \tag{49}$$

$$\frac{-d\rho'}{\rho'} = \frac{\cos\theta \, d\xi}{\rho'} \tag{50}$$

may be used in the integration of 47 and 48 to yield

$$u = \frac{-\gamma}{2\pi} (\theta_2 - \theta_1)$$

$$v = \frac{-\gamma}{2\pi} \ln \frac{\rho'_2}{\rho'_1}$$

The velocity given above is well defined for all field points. However, as a field point approaches the vortex surface from above, the velocity components become

$$u(x, 0_+) = \frac{-\gamma}{2} \tag{51}$$

$$v(x, 0_+) = \frac{-\gamma}{2\pi} \ln \frac{\rho'_2}{\rho'_1} \tag{52}$$

while a field point from below results in velocity components of

$$u(x, 0_-) = + \frac{\gamma}{2} \tag{53}$$

$$v(x, 0_-) = \frac{-\gamma}{2\pi} \ln \frac{\rho'_2}{\rho'_1} \tag{54}$$

Thus it can be seen that there is a discontinuity in the tangential velocity equal to the strength of the vortex sheet.